Physica A 402 (2014) 318–329

Contents lists available at ScienceDirect

Physica A

journal homepage: www.elsevier.com/locate/physa

Noise effect on statistical properties of type-I intermittency

Gustavo Krause [a,b], Sergio Elaskar [a,b,*], Ezequiel del Río [c]

[a] Dpto. de Aeronáutica, Facultad de Ciencias Exactas, Físicas y Naturales, Universidad Nacional de Córdoba, Avenida Vélez Sarsfield 1611 – 5000 Córdoba, Argentina

[b] Consejo Nacional de Investigaciones Científicas y Técnicas (CONICET), Argentina

[c] Dpto. Física Aplicada, ETSI Aeronáuticos, Universidad Politécnica de Madrid, 28040 Madrid, Spain

HIGHLIGHTS

- A new methodology to investigate the noise effect on type-I intermittency is presented.
- The methodology is an extension of other that we recently established for the three classical types of intermittency.
- We consider relatively large noise strengths applied on the reinjection mechanism.
- We show the strong influence of noise in the statistical properties.
- The results are confirmed by numerical simulations.

ARTICLE INFO

Article history:
Received 30 September 2013
Received in revised form 3 February 2014
Available online 12 February 2014

Keywords:
Intermittency
Noise effect
Reinjection probability density

ABSTRACT

In this work we analyze the noise effect on type-I intermittency, for which we develop a methodology based on a recently proposed technique used to model the reinjection probability density (RPD). This new methodology allows us to study the noise effect on the intermittency statistical properties for relatively large noise strengths in a quadratic map with different reinjection mechanisms. We show that this procedure allows to predict the behavior of the noisy and noiseless system using the results of the $M(x)$ function which is implemented to obtain the RPD function. We also derive an analytical approximation for the probability density of the laminar lengths and we obtain results for the average laminar length. All analytical approaches show a good agreement with the numerical results even though the statistical properties are calculated using either the noisy or noiseless data, however in some cases the description of the noiseless system using the noisy data can be inaccurate. In addition, we show that occasionally the presence of noise could be not detected due to the results behave as they would be corresponding to a noiseless system. This aspect may have important consequences especially when working with experimental data.

1. Introduction

Intermittency is a particular route to deterministic chaos, where a transition between regular or laminar and chaotic phases occurs. Pomeau and Manneville introduced the concept of intermittency [1,2]. In the intermittency phenomenon, when a control parameter exceeds a threshold value, the system behavior changes abruptly to a larger attractor by means

* Corresponding author at: Dpto. de Aeronáutica, Facultad de Ciencias Exactas, Físicas y Naturales, Universidad Nacional de Córdoba, Avenida Vélez Sarsfield 1611 – 5000 Córdoba, Argentina. Tel.: +54 351 4334119.
E-mail address: selaskar@efn.uncor.edu (S. Elaskar).

http://dx.doi.org/10.1016/j.physa.2014.02.008
0378-4371/

of an explosive bifurcation [3]. This phenomenon has been observed in several physical topics such as Lorenz system, Rayleigh–Bénard convection, forced nonlinear oscillators, plasma physics, and turbulence [4–7]. Intermittency has been also found in subjects of economical and medical sciences [8,9]. Traditionally, intermittency has been classified into three different types called I, II and III according to the Floquet multipliers or eigenvalue in the local Poincaré map [3,10]. Subsequent studies extended the classification to type X, V, on–off, eyelet and ring intermittencies [11–16].

To generate intermittency, it is necessary to have a reinjection mechanism that maps back the trajectories from the chaotic zone into the local regular or laminar region. This mechanism is described by the reinjection probability density function (RPD), which is defined by the nonlinear dynamics of the system itself. The RPD depends on the global reinjection mechanism.

There are several significant statistical parameters for the intermittent phenomenon description, such as: the probability density of the laminar lengths, the average laminar length and the characteristic relation. In order to calculate these properties, it is necessary to know previously the RPD which determines the reinjection points distribution inside the laminar region. Therefore, the accurate evaluation of the RPD function is very important to correctly describe the intermittency phenomenon. Different approaches to describe the RPD function have been used. The most popular utilized approach is to consider the RPD as a constant function [4,5,10,17,18]. However, this assumption is not applicable for many problems. Also, different approaches have been implemented using a characteristic of the particular nonlinear processes, but these RPD functions cannot be applied for other systems. Recently a more general estimate of the RPD has been introduced [19,20], which includes the uniform reinjection as a particular case.

Since the noise is always present in nature, it is very important to know the effect of noise on the intermittency phenomenon. Many researches devoted to the noise effect on the local Poincaré map have been published for type-I intermittency [17,21–24]. However, there are no studies focused on the noise effect on the RPD function as far as the authors know. It is clear that noise affects the complete zone where the system dynamics takes place. Therefore, the noise effect would modify the RPD. In this paper we present an analytical approach to the noisy reinjection probability density (NRPD) for type-I intermittency. To do this, we extend a recently developed methodology to calculate the NRPD for type-II and III intermittencies [25].

2. Description of the methodology

In this work, we consider a quadratic map to represent the local Poincaré map for type-I intermittency:

$$x_{n+1} = f(x) = a\,x_n^2 + x_n + \varepsilon, \tag{1}$$

where ε is the control parameter which represents the channel width in the laminar region, i.e. the distance between the local Poincaré map and the bisector. The parameter a specifies the position of the point with zero-derivative (we use $a = 1$). In the last equation, for $\varepsilon < 0$ there are two fixed points, one of them stable and the other one unstable. For $\varepsilon = 0$ the two fixed points coalesce in one fixed point $x_0 = 0$ and for $\varepsilon > 0$ there are no fixed points. Furthermore, if there is a reinjection mechanism that maps back the trajectory from the chaotic zone into the local one, type-I intermittency can exist.

In this paper the map implemented in Ref. [26] is used. For that map the nonlinear reinjection mechanism is given by $g(x) = \hat{x} + h\,(x - x_r)^{\gamma}$, where the coefficient h is obtained from the conditions $g(x_r) = \hat{x}$ and $g\,(1) = 1$, where $\hat{x}$ is the lower boundary of reinjection (LBR) which is here considered to be placed inside the laminar interval $[-c, c]$. The point x_r is obtained from $f(x_r) = 1$. The exponent γ permits to obtain different RPD functions. For $\gamma > 1$ the trajectories are concentrated around the LBR point, therefore the RPD has a decreasing structure. On the other hand, for $0 < \gamma < 1$ the trajectories move away from the LBR point and the RPD function has an increasing form. For $\gamma = 1$, the RPD is approximately uniform since the reinjection function $g(x)$ is linear.

Then, the global map can be written as:

$$F(x) = \begin{cases} f(x) = a\,x^2 + x + \varepsilon + \sigma_l \xi_n, & \text{if } x < x_r, \\ g(x) = \hat{x} + \dfrac{1 - \hat{x}}{(1 - x_r)^{\gamma}}\,(x - x_r)^{\gamma} + \sigma_r \xi_n & \text{if } x > x_r. \end{cases} \tag{2}$$

The last terms in Eq. (2) models the noise effect on the system. The variable ξ_n is a random variable which has a uniform probability distribution ("white noise"). We consider that the noise strength is different in each region: σ_l in the local map and σ_r for the reinjection mechanism.

With this configuration we can model a high level noise applied on the reinjection mechanism, where σ_r can be much larger than the control parameter ε, while for the laminar region the condition $\sigma_l < \varepsilon$ is preserved. This is done in order to focus the analysis on the noise effect on the global reinjection, since the condition $\sigma_l < \varepsilon$ ensures that the dynamics of the system at the laminar region is governed by the dynamics of the map. At the end of the paper we change the configuration to show how the presence of high level noise on the local map modifies the results of the probability density of the laminar lengths and produces the saturation phenomenon in the characteristic relation.

Fig. 1 shows the map (2) for three different values of the exponent γ. Also, the noise effect and the LBR point $\hat{x}$ are indicated in this figure.

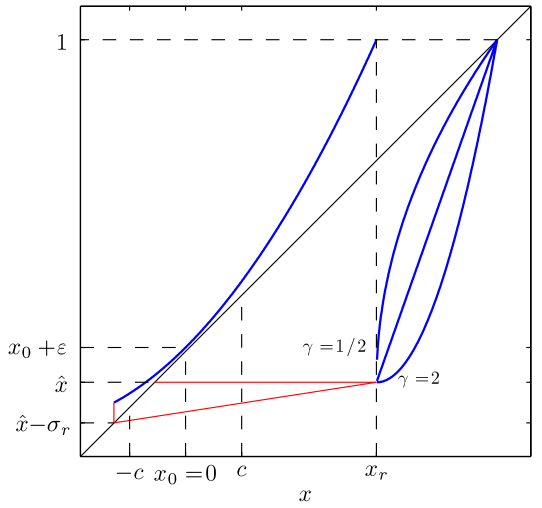

Fig. 1. Map $F(x)$ given by Eq. (2) for different values of exponent γ. The displacement of the LBR point produced by the noise effect is also indicated.

2.1. Analytical approach of the RPD

The RPD function, here denoted by $\phi(x)$, indicates the statistical behavior of the intermittent phenomenon. The calculation of this function is not a simple task. In this work we used the theoretical methodology developed in Refs. [19,20,25,27] to obtain the RPD, which is extended in the following sections to consider the noise effect in type-I intermittency.

In the cited methodology the key point is to use an auxiliary function $M(x)$ to evaluate the RPD instead of directly using the numerical data. Thus, the RPD is evaluated from the $M(x)$ function which is obtained from numerical or experimental data. The function $M(x)$ is defined inside the laminar interval $[-c, c]$ as:

$$M(x) = \begin{cases} \dfrac{\int_{-c}^{x} \tau\, \phi(\tau)\, \mathrm{d}\tau}{\int_{-c}^{x} \phi(\tau)\, \mathrm{d}\tau}, & \text{if } \displaystyle\int_{-c}^{x} \phi(\tau)\, \mathrm{d}\tau \neq 0, \\ 0, & \text{if } \displaystyle\int_{-c}^{x} \phi(\tau)\, \mathrm{d}\tau = 0. \end{cases} \tag{3}$$

Since $M(x)$ is obtained by means of two integrals, this function smooths the experimental or numerical data series and its numerical estimation is more robust than the direct evaluation of the function $\phi(x)$. As $M(x)$ is an average over the reinjection points in the laminar interval, its evaluation is easier than the direct RPD calculation:

$$M(x_q) = \frac{1}{q} \sum_{j=1}^{q} x_j \tag{4}$$

where the reinjection points $\{x_j\}_{j=1}^{N}$ must be previously sorted from the lowest to the highest, i.e. $x_j \leq x_{j+1}$.

For a wide class of maps exhibiting type-I intermittency without noise, the function $M(x)$ satisfies a linear approximation when the LBR point is placed inside the laminar interval $(-c \leq \hat{x} < c)$ [26]:

$$M(x) = m\left(x - \hat{x}\right) + \hat{x}, \tag{5}$$

where the slope of the straight line is $0 < m < 1$. Then, the RPD function can be written as [19]:

$$\phi(x) = b\left(x - \hat{x}\right)^{\alpha}, \tag{6}$$

where b is a normalization parameter, and

$$\alpha = \frac{2m - 1}{1 - m} \tag{7}$$

being $\alpha > -1$ because $0 < m \leq 1$.

The LBR limit $(\hat{x})$ is a critical point of the RPD function, where $\phi(\hat{x}) \to \infty$ for $\alpha < 0$, and $\phi(\hat{x}) \to 0$ if $\alpha > 0$. The specific case verifying $\alpha = 0$ $(m = 1/2)$ corresponds to the uniform reinjection $\phi(x) = \text{const}$.

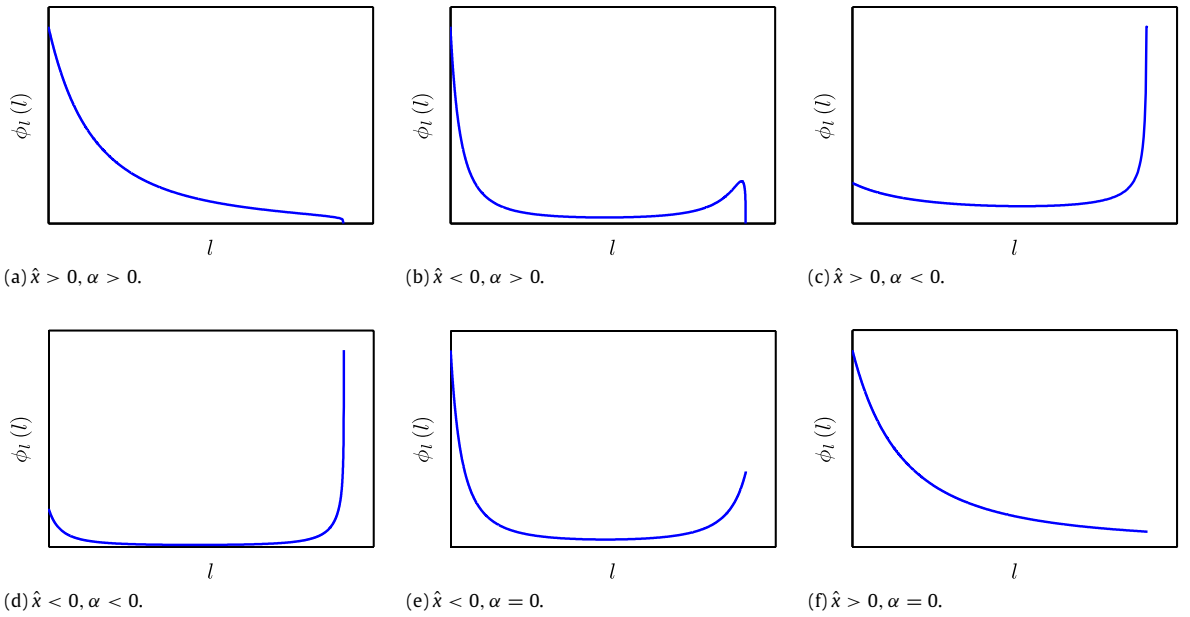

(a) $\hat{x} > 0, \alpha > 0$. (b) $\hat{x} < 0, \alpha > 0$. (c) $\hat{x} > 0, \alpha < 0$.

(d) $\hat{x} < 0, \alpha < 0$. (e) $\hat{x} < 0, \alpha = 0$. (f) $\hat{x} > 0, \alpha = 0$.

Fig. 2. Probability density of the laminar lengths $\phi_l(l)$ for several parameters $\hat{x}$ and α.

2.2. The probability density of the laminar lengths

The laminar length counts the number of iterations spent by a trajectory inside the laminar interval. In the noiseless case it depends only on the local map. However, to take in consideration the reinjection mechanism it is used the probability density of the laminar lengths $\phi_l(l)$. This function defines the probability of finding a given laminar length.

The local Poincaré map given by Eq. (1) with $\sigma_l = 0$ is used to evaluate the noiseless laminar length. Under the assumption $\varepsilon \to 0$, the discrete equation $x_{n+1} - x_n$ can be approximated by the following differential equation [10]:

$$\frac{\mathrm{d}x}{\mathrm{d}l} = a\,x^2 + \varepsilon. \tag{8}$$

The solution of the last equation inside the interval $[-c, c]$ results:

$$l(x, c) = \int_x^c \frac{1}{a\,x^2 + \varepsilon}\,\mathrm{d}x = \frac{1}{\sqrt{a\varepsilon}}\left[\tan^{-1}\left(\sqrt{\frac{a}{\varepsilon}}c\right) - \tan^{-1}\left(\sqrt{\frac{a}{\varepsilon}}x\right)\right]. \tag{9}$$

Then, for type-I intermittency, the probability of finding a laminar length between l and $l + \mathrm{d}l$ is [10]:

$$\phi_l(l) = \phi[X(l, c)]\left|\frac{\mathrm{d}X(l, c)}{\mathrm{d}l}\right| = \phi[X(l, c)]\left|a\,[X(l, c)]^2 + \varepsilon\right|, \tag{10}$$

where $X(l, c)$ is the inverse function of $l(x, c)$ given by Eq. (9), which can be written as:

$$X(l, c) = \sqrt{\frac{\varepsilon}{a}}\tan\left[\tan^{-1}\left(\sqrt{\frac{a}{\varepsilon}}c\right) - \sqrt{a\varepsilon}\,l\right]. \tag{11}$$

Note that the features of the function $\phi_l(l)$ depend on the parameters $\hat{x}$ and α (see Eq. (6)). Fig. 2 shows the different form for the probability density of the laminar lengths in type-I intermittency [26].

Fig. 2(b) shows that for some values of the parameters $\hat{x}$ and α, the function $\phi_l(l)$ can have a local maximum. This fact can be used in an experimental case to identify the unknown parameters of the system from the shape of $\phi_l(l)$. Note, however, that in experiments the noise is always present, therefore in the next section we study the noise effect showing that the referred maximum still appears in presence of noise but for shifted parameters values.

The results for $\phi_l(l)$ obtained in this section can be extended for the noisy case only when the condition $\sigma_l < \varepsilon$ is verified, because for $\sigma_l \gg \varepsilon$ the differential approximation carried out in Eq. (8) cannot be performed.

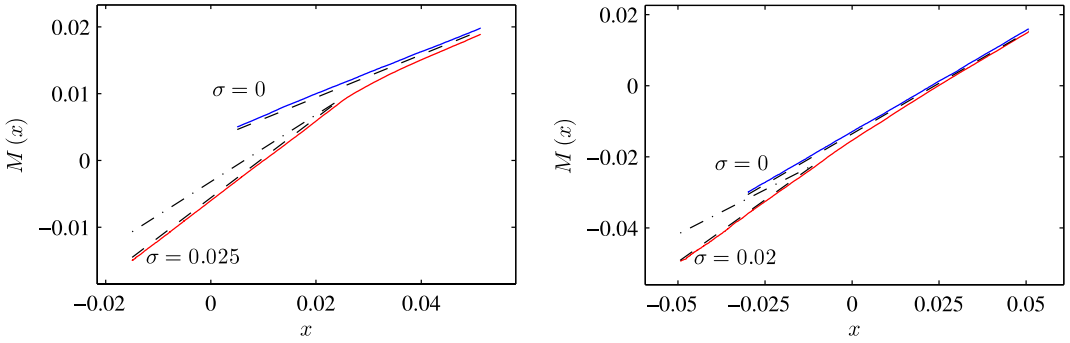

(a) $\hat{x} = 0.005$, $\gamma = 2$. (b) $\hat{x} = -0.03$, $\gamma = 0.75$.

Fig. 3. Comparison between the noisy and noiseless $M(x)$ functions with $\varepsilon = 10^{-4}$, $c = 0.05$ and the indicated values. Dashed lines show the slope of the linear regions of functions $M(x)$. The slopes are $m = 0.320$ ($\alpha = -0.529$) and $m_1 = 0.595$ ($\alpha_1 = 0.469$) for (a), and $m = 0.570$ ($\alpha = 0.326$) and $m_1 = 0.698$ ($\alpha_1 = 1.311$) for (b). In both cases $\alpha_1 \approx \alpha + 1$. Also, note that for the largest values of x the slopes are quite similar. The slope of the dashed-dot line is 1/2 indicating the slope of uniform reinjection.

3. Noise effect in type-I intermittency

We have seen that when the noiseless model is considered and the $\hat{x}$ limit belongs to the laminar interval, we have a continuous RPD function whose form depends on the value of exponent γ in the return function $g(x)$ (see Eq. (2)). In this case the RPD is obtained using the $M(x)$ function following the previous work [26].

In the following sections we present the noise effect on type-I intermittency considering map (2) for $\varepsilon > \sigma_l \to 0$. This condition does not affect the results relating to the function $M(x)$ and the RPD, since they only depend on the global reinjection mechanism. However, as we will see later, this has significant consequences on $\phi_l(l)$ and the characteristic relation.

The noise presence not only produces changes in the RPD due to the redistribution of reinjection points, but also it generates the displacement of the $\hat{x}$ point, which is located in the new position $\hat{x} - \sigma_r$ (see Fig. 1). This displacement modifies the associated $\phi_l(l)$ function with respect to the noiseless results shown in Fig. 2 for different values of $\hat{x}$ and α. In addition, if this displacement is such that $\hat{x} - \sigma_r < -c$, a discontinuity in the RPD function appears and consequently the $M(x)$ function will not be linear. A detailed analysis of this situation is made in a paper where we extend the previously presented approach to consider the case of arbitrary shapes of $M(x)$ [28].

Following Ref. [25] it can be observed that the associated power law to the RPD for the noiseless map appears to be robust against noise, hence the noiseless density $\phi(x)$ should be transformed into a new density $\Phi(x)$ according to the convolution

$$\Phi(x) = \int_{-\infty}^{\infty} \phi(z)\, G(x - z, \sigma_r)\ \mathrm{d}z, \tag{12}$$

where $G(x - z, \sigma_r)$ is the probability density of the noise term $\sigma_r \xi_n$ in Eq. (2).

As noise source we use a random variable ξ_n in the interval $[-1, 1]$, hence the probability density G in Eq. (12) results:

$$G(x, \sigma_r) = \frac{\Theta(x + \sigma_r) - \Theta(x - \sigma_r)}{2\sigma_r}, \tag{13}$$

where Θ is the well known Heaviside step function. Finally, after integrating Eq. (12), we get the NRPD as

$$\Phi(x) = \frac{b}{2\sigma_r\,(\alpha + 1)} \left\{ \left[x - \left(\hat{x} - \sigma_r\right)\right]^{\alpha+1} - \Theta\left[x - \left(\hat{x} + \sigma_r\right)\right] \left[x - \left(\hat{x} + \sigma_r\right)\right]^{\alpha+1} \right\}. \tag{14}$$

Note that in Eq. (14) the position of the LBR is shifted to a new position given by $\left(\hat{x} - \sigma_r\right)$. In view of this, we split our analysis in two cases according to $\hat{x} - \sigma_r > -c$ or $\hat{x} - \sigma_r < -c$.

In the first case, $\hat{x} - \sigma_r > -c$, the function $g(x)$ reinjects all trajectories directly into the laminar zone and the function $M(x)$ can be approximated by a piecewise linear function as Fig. 3 shows. This shape is a consequence of expression (14). Note that for $x < \hat{x} + \sigma_r$ the Heaviside function is zero and we recover for $\Phi(x)$ the same power law that for $\phi(x)$ but the parameters are shifted from $\hat{x}$ to $\hat{x} - \sigma_r$ and from α to $\alpha + 1$, consequently, Eq. (5) now can be written as

$$M(x) = m_1 \left(x - \hat{x}_1\right) + \hat{x}_1, \quad x < \hat{x} + \sigma_r, \tag{15}$$

where $\hat{x}_1 = \hat{x} - \sigma_r > -c$. By fitting the data plotted in Fig. 3(a) in the region $x < \hat{x} + \sigma_r = 0.03$ we get $\hat{x}_1 \approx -0.01997$, very close to the exact value used in the numerical simulation $\hat{x} - \sigma_r = -0.02$.

On the other hand, for $x > \hat{x} + \sigma_r$, and for small values of σ_r we can approximate $\Phi(x)$ in Eq. (14) by

$$\Phi(x) \approx \frac{\mathrm{d}}{\mathrm{d}x} b \left(x - \hat{x}\right)^{\alpha+1}, \tag{16}$$

hence in that region the exponent of $\Phi(x)$ approximates to the exponent of the noiseless density given by Eq. (6). Note that according to Eq. (7), the two slopes of $M(x)$, m_1 and m_2, corresponding to the regions with exponents $\alpha+1$ and α respectively, are related by

$$m_1 = \frac{1}{2-m_2}. \tag{17}$$

To check the last expression, we evaluate in Fig. 3(a) m_1 and m_2 by fitting the data in two regions on each side of $x = 0.03$. To obtain m_1 all points $x < 0.03$ are used, but for m_2 it must be considered that the transition between the slopes is smooth rather than sharp, hence we use points $x \to c$ where the slope of the function $M(x)$ is more similar to the noiseless one. The value obtained for m_2 is $m_2 \approx 0.3327$, then Eq. (17) provides the value $m_1 \approx 0.599772$ very close to 0.5954 obtained by fitting the numerical data.

Furthermore, it is possible to estimate not only $\hat{x}_1$ but also its components $\hat{x}$ and σ_r. That is, we can separate the noise component from the noiseless parameters. To do this we approximate $C_2 \approx \hat{x}+\sigma$, where C_2 is the intersection point between the two straight lines fitting the piecelinear function $M(x)$. With this approximation we have

$$\hat{x} = \frac{C_2+\hat{x}_1}{2} \quad \text{and} \quad \sigma_r = \frac{C_2-\hat{x}_1}{2}. \tag{18}$$

In the case of Fig. 3(a) we have from Eq. (18) $\hat{x} \approx 0.00731974$ and $\sigma_r \approx 0.0272901$. Note that in this case, the approximation overestimates the real values ($\hat{x} = 0.005$ and $\sigma_r = 0.025$). This is due to the smooth transition from slope m_1 to m_2 aforementioned, which is produced by the memory effect provided by the integrals in the definition of $M(x)$.

The previously detailed behavior was verified by several simulations for different values of the parameters $(\varepsilon, \hat{x}, \gamma, \sigma_r)$. This implies that the slope of the noisy region of $M(x)$ does not depend on the noise strength, but is defined by the form of the return function (exponent γ) which governs the behavior of the noiseless $M(x)$. In this manner, we can obtain the exponent α when the noiseless data is not available, either using the expression $\alpha = \alpha_1 - 1$ where α_1 is calculated from the slope m_1, or via the slope m_2 of $M(x)$ at the end of the laminar interval.

Eq. (14) models the noise effect on the reinjection points distribution for $\hat{x} - \sigma_r > -c$. When the displacement of the LBR limit goes beyond the left end of the laminar interval ($\hat{x} - \sigma_r < -c$) a jump discontinuity appears in the NRPD, which is located in the point $x_c = F(-c)$. This occurs because the displacement $\hat{x} - \sigma_r$, below $-c$, generates that the trajectories going through points $x < -c$ always reinject in the region $x < x_c$, which produces a concentration of reinjection points in the sub-interval $\left[\hat{x}_2, x_c\right)$, where the point $\hat{x}_2$ is the lowest reinjection point of orbits passing through $x < -c$. A more detailed discussion about this discontinuity is made in Ref. [28].

The limit $\hat{x}_2$ of the sub-interval where the concentration of reinjection points is produced depends on the noise strength: for $F\left(\hat{x}-\sigma_r\right) < -c$, $\hat{x}_2 \equiv -c$, on the contrary for $F\left(\hat{x}-\sigma_r\right) > -c$, $\hat{x}_2 \equiv F\left(\hat{x}-\sigma_r\right)$.

Considering only points $\hat{x}_2 \le x < x_c$, an approximately linear noisy function $M(x)$ is always observed in that region. Hence, we can assume a solution of the form:

$$\phi_k(x) = bk\left(x-\hat{x}_2\right)^{\alpha_k}, \quad \hat{x}_2 \le x < x_c, \tag{19}$$

where b is the normalization parameter and the exponent α is calculated with Eq. (7) using the slope of $M(x)$ for points $\hat{x}_2 \le x < x_c$. The coefficient k weighs the difference of proportion between the reinjection points coming from $x < -c$ and those coming from $g(x)$.

The function $\phi_k(x)$ is defined in the sub-interval $\left[\hat{x}_2, x_c\right)$. It is added to the solution (14) in that region in order to incorporate both effects in the NRPD, namely, the effect of re-distribution of the reinjection points due to noise and the effect of concentration in the left end of the laminar interval. For $\hat{x} - \sigma_r > -c$ there is no concentration, therefore $k = 0$ and then $\phi_k(x) = 0$.

Finally, the NRPD function $\Phi(x)$ results:

$$\Phi(x) = \begin{cases} \dfrac{b}{2\sigma_r(\alpha+1)}\left\{\left[x-\left(\hat{x}-\sigma_r\right)\right]^{\alpha+1} - \Theta\left[x-\left(\hat{x}+\sigma_r\right)\right]\left[x-\left(\hat{x}+\sigma_r\right)\right]^{\alpha+1}\right\} \\ \quad + bk\left(x-\hat{x}_2\right)^{\alpha_k}, \quad \text{if } \hat{x}_2 \le x < x_c, \\ \dfrac{b}{2\sigma_r(\alpha+1)}\left\{\left[x-\left(\hat{x}-\sigma_r\right)\right]^{\alpha+1} - \Theta\left[x-\left(\hat{x}+\sigma_r\right)\right]\left[x-\left(\hat{x}+\sigma_r\right)\right]^{\alpha+1}\right\}, \quad \text{otherwise}, \end{cases} \tag{20}$$

where the normalization parameter b is obtained such that $\int_{x_{j\min}}^{c} \Phi(x)\ \mathrm{d}x = 1$, being $x_{j\min}$ the lowest reinjection point given by the greater of $\hat{x}-\sigma_r$ and $-c$. The calculation of the coefficient k is performed using the definition of function $M(x)$ as described below.

From Eqs. (3) and (20), for points $x > x_c$ the function $M(x)$ is:

$$M(x) = \frac{\frac{1}{2\sigma_r(\alpha+1)}\int_{x_{j\min}}^{x} \tau\left[\left(\tau-\hat{x}+\sigma_r\right)^{\alpha+1} - \Theta\left(\tau-\hat{x}-\sigma_r\right)\left(\tau-\hat{x}-\sigma_r\right)^{\alpha+1}\right]\mathrm{d}\tau + k\int_{\hat{x}_2}^{x_c}\tau\left(\tau-\hat{x}_2\right)^{\alpha_k}\mathrm{d}\tau}{\frac{1}{2\sigma_r(\alpha+1)}\int_{x_{j\min}}^{x}\left[\left(\tau-\hat{x}+\sigma_r\right)^{\alpha+1} - \Theta\left(\tau-\hat{x}-\sigma_r\right)\left(\tau-\hat{x}-\sigma_r\right)^{\alpha+1}\right]\mathrm{d}\tau + k\int_{\hat{x}_2}^{x_c}\left(\tau-\hat{x}_2\right)^{\alpha_k}\mathrm{d}\tau},$$

which gives

$$M(x) = \frac{\frac{1}{2\sigma_r(\alpha+1)(\alpha+2)(\alpha+3)}\left\{\left(x-\hat{x}+\sigma_r\right)^{\alpha+2}\left[x(\alpha+2)+\hat{x}-\sigma_r\right]-\left(x_{j\min}-\hat{x}+\sigma_r\right)^{\alpha+2}\left[x_{j\min}(\alpha+2)+\hat{x}-\sigma_r\right]-\Theta\left(x-\hat{x}-\sigma_r\right)\left(x-\hat{x}-\sigma_r\right)^{\alpha+2}\left[x(\alpha+2)+\hat{x}+\sigma_r\right]\right\}+\frac{k}{(\alpha_k+1)(\alpha_k+2)}\left(x_c-\hat{x}_2\right)^{\alpha_k+1}\left[x_c(\alpha_k+1)+\hat{x}_2\right]}{\frac{\left(x-\hat{x}+\sigma_r\right)^{\alpha+2}-\left(x_{j\min}-\hat{x}+\sigma_r\right)^{\alpha+2}-\Theta\left(x-\hat{x}-\sigma_r\right)\left(x-\hat{x}-\sigma_r\right)^{\alpha+2}}{2\sigma_r(\alpha+1)(\alpha+2)}+\frac{k}{(\alpha_k+1)}\left(x_c-\hat{x}_2\right)^{\alpha_k+1}}. \quad (21)$$

The numerical values of $M(x)$ are known, therefore the k coefficient can be evaluated in terms of the other parameters, which are also known. Then, considering points $x > x_c$ results:

$$k = \frac{\left(x-\hat{x}+\sigma_r\right)^{\alpha+2}\left[M(x)-\frac{x(\alpha+2)+\hat{x}-\sigma_r}{(\alpha+3)}\right]+\left(x_{j\min}-\hat{x}+\sigma_r\right)^{\alpha+2}\left[\frac{\hat{x}(\alpha+3)-\sigma_r}{(\alpha+3)}\right]+\Theta\left(x-\hat{x}-\sigma_r\right)\left(x-\hat{x}-\sigma_r\right)^{\alpha+2}\left[\frac{x(\alpha+2)+\hat{x}+\sigma_r}{(\alpha+3)}-M(x)\right]}{\frac{2\sigma_r(\alpha+1)(\alpha+2)}{(\alpha_k+1)(\alpha_k+2)}\left(x_c-\hat{x}_2\right)^{\alpha_k+1}\left[x_c(\alpha_k+1)+\hat{x}_2-M(x)(\alpha_k+2)\right]}. \quad (22)$$

Finally the normalization parameter is obtained to complete all required values.

$$b = \left[\frac{\left(c-\hat{x}+\sigma_r\right)^{\alpha+2}-\left(x_{j\min}-\hat{x}+\sigma_r\right)^{\alpha+2}-\Theta\left(c-\hat{x}-\sigma_r\right)\left(c-\hat{x}-\sigma_r\right)^{\alpha+2}}{2\sigma_r(\alpha+1)(\alpha+2)}+\frac{k}{(\alpha_k+1)}\left(x_c-\hat{x}_2\right)^{\alpha_k+1}\right]^{-1}. \quad (23)$$

4. Numerical results and comparison with the proposed theory

For the analytical approach of the noisy probability density of laminar lengths $\Phi_l(l)$, under the assumption $\varepsilon > \sigma_l \to 0$, we can use Eq. (10) where $\phi[X(l,c)]$ is replaced by its noisy version $\Phi[X(l,c)]$ and, taking into account that the noise effect is included in the NRPD, $X(l,c)$ is evaluated using Eq. (11).

In the next figures we show the results for different values of ε, $\hat{x}$, γ and σ_r with $c = 0.05$. In these figures the numerical data (blue points) and the analytical approximation (red lines) are compared. We also show the corresponding noiseless results in order to clearly observe the effect of noise.

In Figs. 4 and 5 a very good agreement between the numerical data and the analytical approach can be observed for both, the NRPD and the probability density of the laminar lengths $\Phi_l(l)$. It can also be seen that the strong influence of noise in the form of the functions $\Phi(x)$, $\Phi_l(l)$ and in the leak of linearity of $M(x)$. In the case of Fig. 4, the feature $\phi(\hat{x}) \to \infty$ is replaced by $\phi(\hat{x}-\sigma_r) \to 0$ due to the noise presence, which also affects the density Φ_l that behaves as if would be $\alpha > 0$ with $\hat{x} < 0$ in the noiseless case (see Fig. 2(b)). On the other hand, functions $\Phi(x)$ and $\Phi_l(l)$ in Fig. 5 exhibit the discontinuity described in the previous section because $\hat{x}-\sigma_r < -c$. The jump in the probability density of the laminar lengths occurs at point corresponding to the maximum laminar length $l(-c,c)$ since all points going through interval $[-c, x_c]$ need the same number of iterations to leave the laminar region.

In addition, we can see in Fig. 4 that the relation $m_1 \approx 1/(2-m)$ between the slopes of the noisy and noiseless functions $M(x)$ is verified. This relation have significant implications because the combination of the displacement of the LBR with the increasing of the α by one unity can produce that the exponent changes from negative to positive values due to noise. This indicates that one could confuse a noisy linear $M(x)$ function with a noiseless one, whose true noiseless exponent α is $\alpha - 1$ instead. This situation is shown in Fig. 6, where we can see that the noisy and noiseless cases produce very similar results although their parameters are very different.

4.1. Characteristic relations

In this section we carry out the analysis of the noise influence on the noiseless characteristic relation $\langle l\rangle \propto \varepsilon^{\beta}$, which relates the average laminar length $\langle l\rangle$ to the control parameter ε through the critical exponent β.

The average laminar length depends on the laminar length and the reinjection probability density $\Phi(x)$:

$$\langle l\rangle = \int_{-c}^{c} \Phi(x)\, l(x,c)\, \mathrm{d}x. \quad (24)$$

From previous results and knowing that inside the sub-interval $[-c, x_c)$ the laminar length is equal to the maximum laminar length $l(-c,c)$ when $\varepsilon > \sigma_l \to 0$, we can write:

$$\langle l\rangle \approx \int_{-c}^{c} \Phi'(x)\, l(x,c)\, \mathrm{d}x + l(-c,c)\int_{-c}^{x_c} \phi_k(x)\, \mathrm{d}x, \quad (25)$$

where $\Phi'(x)$ is the NRPD function of Eq. (14) considering only the effect of re-distribution points by noise. For $\hat{x}-\sigma_r > -c$ is $\phi_k(x) = 0$ and the lower limit of the first integral of Eq. (25) is $\hat{x}-\sigma_r$, because $\Phi'(x) = 0$ for $x < \hat{x}-\sigma_r$. On the contrary the last equation results:

$$\langle l\rangle = \frac{b}{2\sigma_r(\alpha+1)}\int_{-c}^{c}\left[\left(x-\hat{x}+\sigma_r\right)^{\alpha+1}-\Theta\left(x-\hat{x}-\sigma_r\right)\left(x-\hat{x}-\sigma_r\right)^{\alpha+1}\right] l(x,c)\, \mathrm{d}x + \frac{bk}{(\alpha_k+1)}\left(x_c-\hat{x}_2\right)^{\alpha_k+1} l(-c,c) \quad (26)$$

where the first integral does not have an analytical solution and then must be numerically solved.

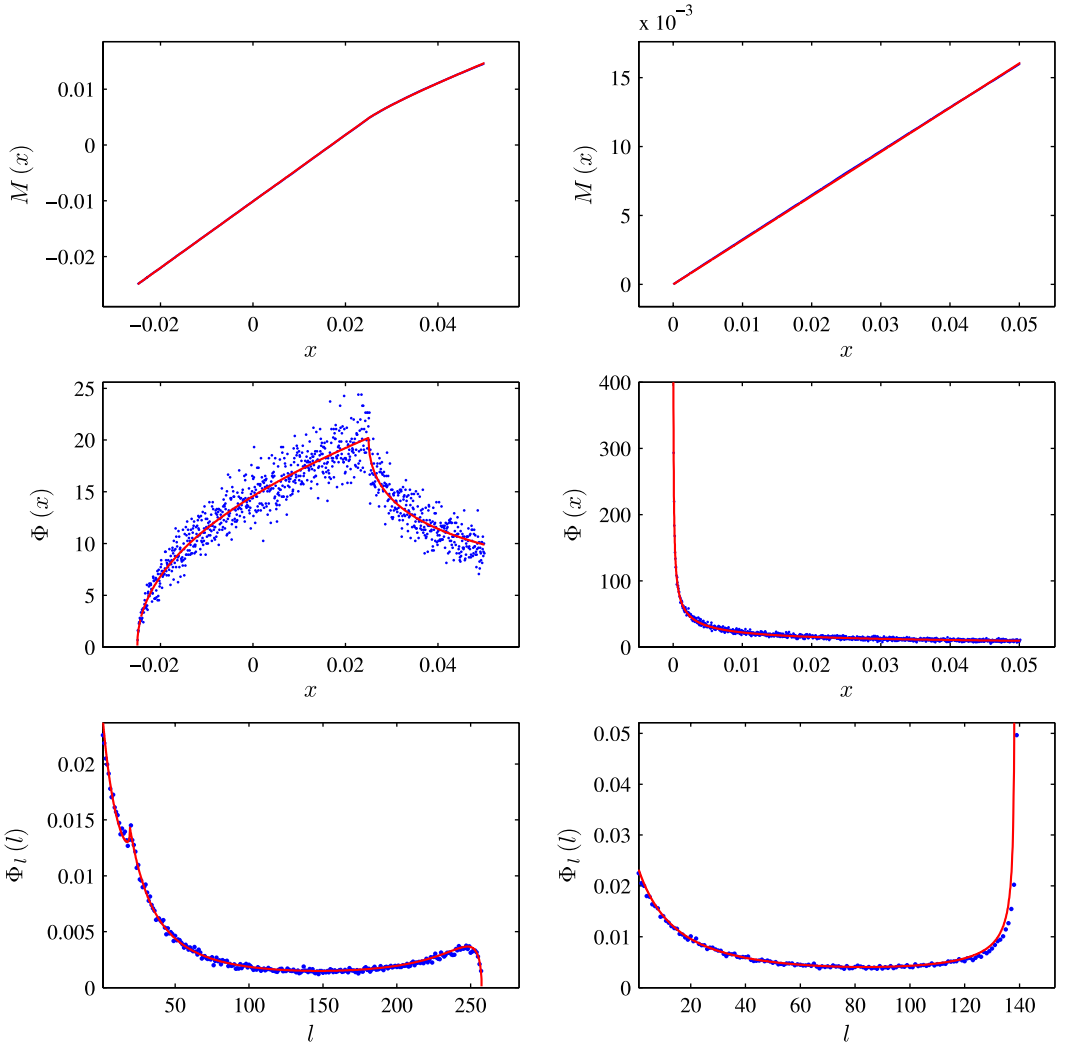

(a) $\sigma_r = 0.025$. (b) $\sigma_r = 0$.

Fig. 4. $M(x)$, NRPD and probability density of laminar lengths for map (2) with $\varepsilon = 10^{-4}, \hat{x} = 0, \gamma = 2, c = 0.05$ and the indicated noise levels. The slopes are $m = 0.320$ ($\alpha = -0.529$) for the noiseless case, $m_1 = 0.596$ ($\alpha_1 = 0.479$) and $m_2 = 0.331$ ($\alpha_2 = -0.505$) for the noisy $M(x)$ in each linear region. Because $\hat{x} - \sigma_r > -c$ in this case the concentration coefficient is $k = 0$.

Fig. 7 shows log–log plots of the characteristic relation $\langle l \rangle \propto \varepsilon^{\beta}$ for different noise levels σ_r and different combinations of values $\hat{x}$ and γ. In the figure the blue circles represent the numerical data and the red crosses the analytical approach of Eq. (26). The solid lines indicate the slope β of the characteristic relation. In addition, dashed lines are placed to show the variation of the maximum laminar length $l(-c, c)$.

According to Kim et al. [18], the value of the exponent β for $\varepsilon \to 0$ depends on the position of point $\hat{x}$: for $\hat{x} \approx -c$ the exponent $\beta \to -1/2$, while for $\hat{x} > 0$ is $\beta = 0$, with a transition of the critical exponent from $-1/2$ to 0 via $\beta = -1/4$ for $\hat{x} = 0$. In Fig. 7(a) and (b) it is observed that the noise influence on the characteristic relation is mainly due to the displacement of the LBR point, which produces the change of the critical exponent β, modifying the shape of the characteristic relation. On the other hand, for $\hat{x} \approx -c$, noise produces a displacement of the curve $\langle l \rangle$ which does not change its shape. The displacement is in the direction of the maximum laminar length $l(-c, c)$, keeping $\beta \approx 1/2$, as observed in Fig. 7(c) and (d). It must be highlighted that the described changes are independent on the NRPD form and they are only defined by the position of the point LBR and the noise strength.

The previously presented results are valid for the condition $\varepsilon > \sigma_l \to 0$. If we relax this restriction the results are the same for $M(x)$ and the RPD since they only depend on the global reinjection mechanism no matter what happens in the local map. However, the influence of the noise strength in the laminar region is mandatory, as explained below.

When $\sigma_l > \varepsilon$ the dynamics of the system in the laminar region is governed by noise because the movement of the orbits is driven by the action of noise. This can produce that newly reinjected trajectories rapidly leave the laminar interval

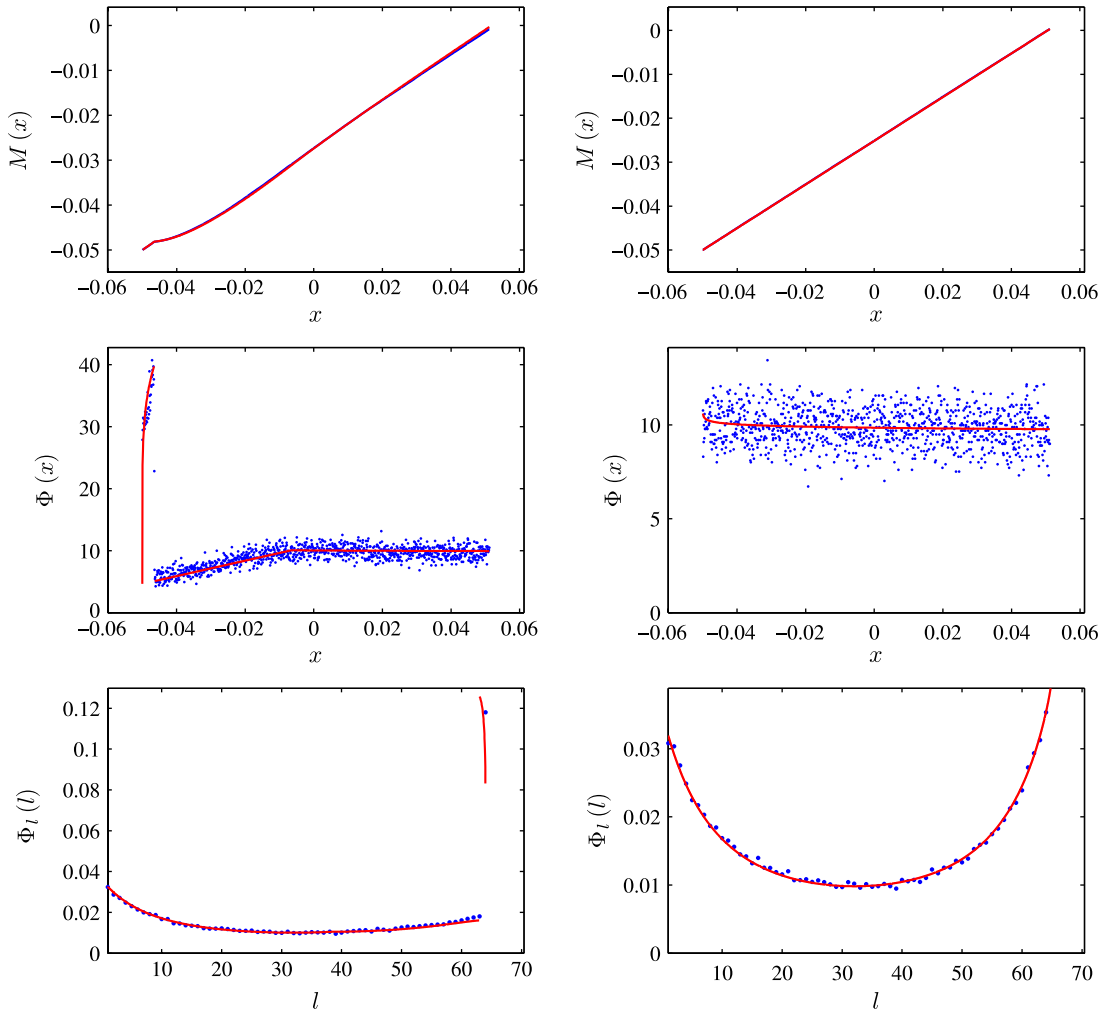

(a) $\sigma_r = 0.04$. (b) $\sigma_r = 0$.

Fig. 5. As Fig. 4 with $\varepsilon = 10^{-3}, \hat{x} = -0.05, \gamma = 1$ and $c = 0.05$. In this case is $\alpha = -0.011$ (approximately uniform RPD for the noiseless case). The relations between α and α_1 cannot be made because $M(x)$ is not linear due to the discontinuity in the NRPD. The concentration coefficient is $k = 7.885$.

regardless where they have reinjected. On the other hand, a sequence of positive and negative deviations caused by high level noise could produce that an orbit indefinitely remains inside the laminar region. Consequently the function $\Phi_l(l)$ does not depend on the parameters of the map when $\sigma_l \gg \varepsilon$, but it has always the same exponentially decreasing shape generated by the high probability that a laminar phase rapidly leaves the laminar region due to the strong noise and the almost zero possibility that an orbit infinitely remains in that region. In Fig. 8 we show the results of $\Phi_l(l)$ for different noise levels applied on the whole map for the cases of Figs. 4 and 5. We can observe that there is a transition between the noiseless result and the exponentially decreasing $\Phi_l(l)$ in which a local maximum is registered. In case of Fig. 8(a) this maximum is due to the displacement of the LBR as happened in Fig. 4, while for Fig. 8(b) the local maximum is a consequence of the noise in the local map that smooths the discontinuity which should appear similarly to Fig. 5 if $\sigma_l \ll \varepsilon$. Beyond the behavior of the transition in each case, we can observe that the results for $\sigma_l \gg \varepsilon$ are very similar in spite of the parameters that are used.

With respect to the characteristic relation, we can see that when a high level of noise is considered in the laminar region, we obtain similar results to those obtained in the analysis of noise effect for types II and III intermittencies, carried out in Ref. [25]. In that case the presence of noise generates a saturation for $\varepsilon \to 0$, which is produced because the time escape due to the dynamics of the map is greater than the time random escape when $\sigma_l > \varepsilon$. As a consequence of saturation, the average laminar length reaches a constant limit value which depends on the noise strength σ_l. The characteristic relations in log–log plots are shown in Fig. 9 for different values of noise strength and exponents γ, which produces different shapes of the NRPD functions. In this figure only numerical data is shown because the analytical expressions (9) and (11) involved in the calculation of $\langle l \rangle$ are not valid due to the noise presence in the laminar region.

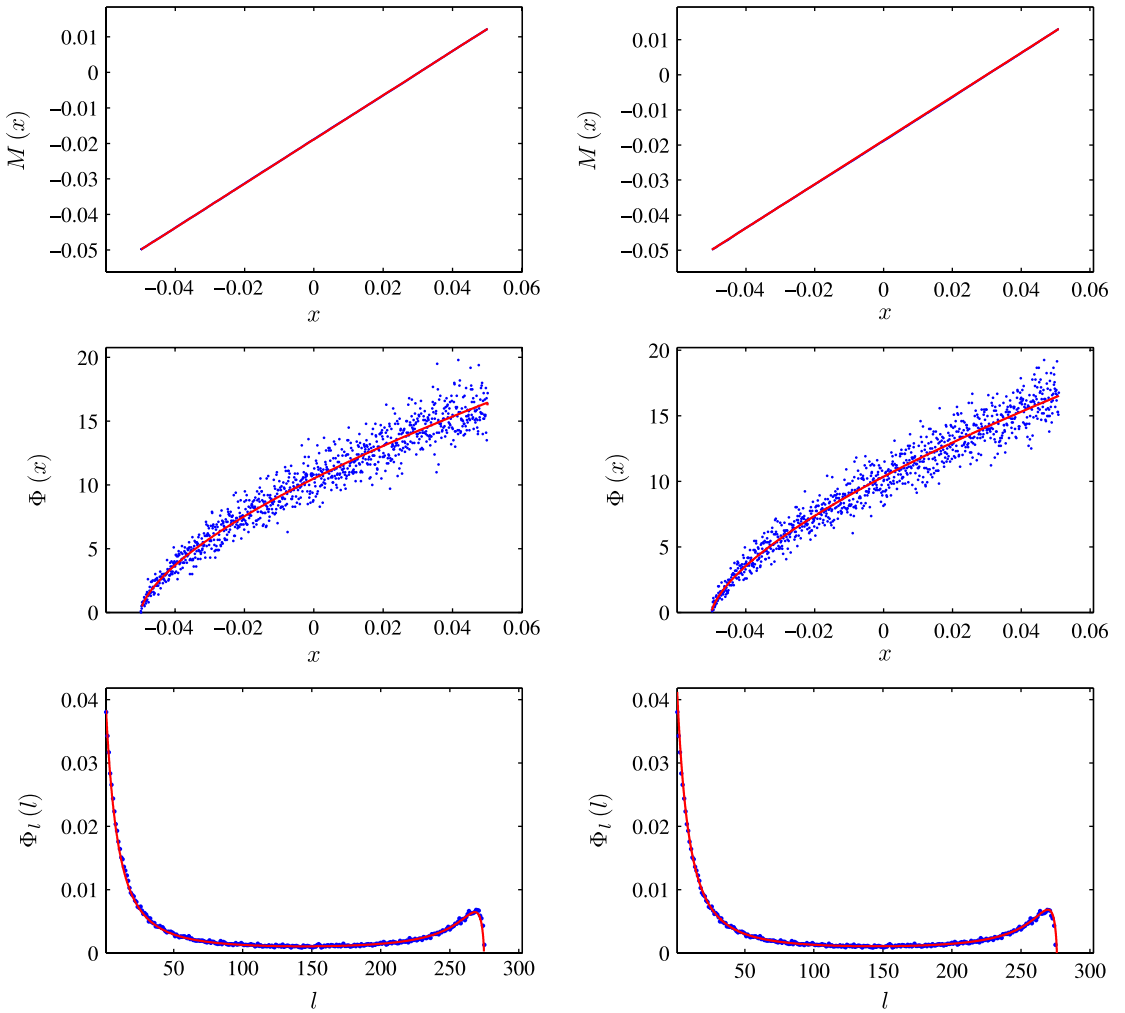

(a) $\gamma = 0.60$, $\hat{x} = 0$ and $\sigma_r = 0.05$.

(b) $\gamma = 1.50$, $\hat{x} = -0.05$ and $\sigma_r = 0$.

Fig. 6. $M(x)$, NRPD and probability density of laminar lengths for map (2) with $\varepsilon = 10^{-4}$, $c = 0.05$ and the indicated values. The results are very similar for both cases: the slope of the noisy $M(x)$ is $m_1 = 0.623$ ($\alpha_1 = 643$) and for the noiseless case $m = 0.624$ ($\alpha = 665$).

It can be observed in the figure that the saturation is produced in the same way as described in Ref. [25], but unlike those results for type-II and III intermittencies, in this case the characteristic relation only depends on the noise strength and is not affected by the form of the NRPD, in according to Refs. [21,24].

An important result of this analysis is that, similarly to the results with $\sigma_l < \varepsilon$, the presence of noise strongly modifies the expected forms for both, the probability density of the laminar lengths and the characteristic relation. As a result, the shapes of $\Phi_l(l)$ and $\langle l \rangle$ does not depend on the parameters $\hat{x}$ and α in according to Fig. 2 and the conclusions of Ref. [18], but they have always the same form which would suggest that the parameters of the system are $\hat{x} > 0$ and $\alpha \leq 0$.

5. Conclusions

In this work we have extended a recently proposed methodology [19,20] used to analyze the intermittency phenomenon, in order to study the noise effect on type-I intermittency. Although there are certainly many papers devoted to the analysis of noise effect on the laminar region, to our knowledge, the noise effect on the reinjection probability density has not been fully considered.

In this paper we obtained an analytical approach to the noisy reinjection probability density (NRPD). The employed methodology is based on the $M(x)$ function, whose results showed that in type-I intermittency, contrary to the type-II and III cases [25], we can predict the behavior of the noisy and noiseless RPD only using the results of this function. Furthermore, when the strength of the noise applied on the laminar region is smaller than the control parameter, the analytical description of the NRPD allowed to model the noise effect on the probability density of the laminar lengths and the average laminar

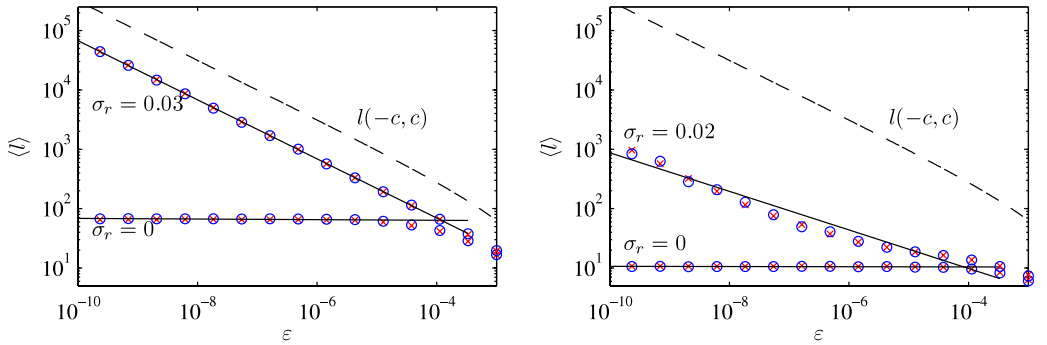

(a) $\hat{x} = 0.005$, $\gamma = 2$.

(b) $\hat{x} = 0.01$, $\gamma = 0.5$.

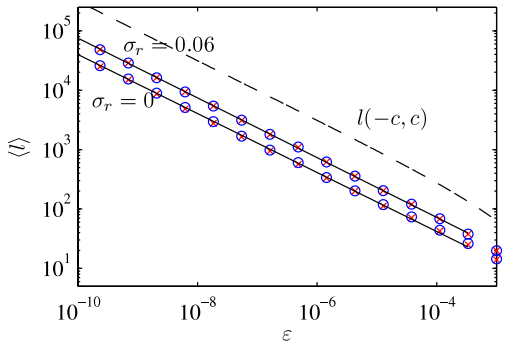

(c) $\hat{x} = -0.04$, $\gamma = 0.4$.

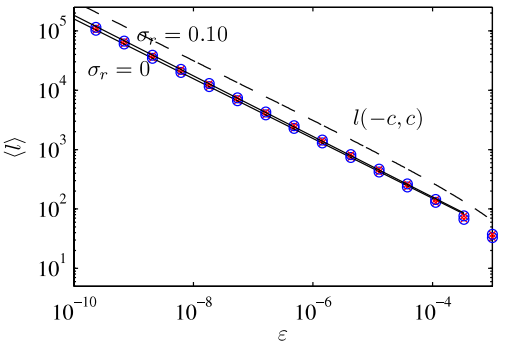

(d) $\hat{x} = -0.05$, $\gamma = 1$.

Fig. 7. Characteristic relation $\langle l \rangle \propto \varepsilon^{\beta}$ for the map (2) with $c = 0.05$ and the indicated values. The noisy critical exponent of case (b) is $\beta \approx -0.32$ showing the transition that takes place for $\hat{x} - \sigma_r \approx 0$.

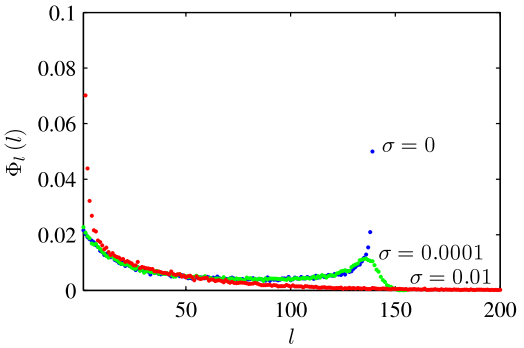

(a) $\varepsilon = 10^{-4}$, $\gamma = 2$, $\hat{x} = 0$, $\sigma_l = \sigma_r = \sigma$.

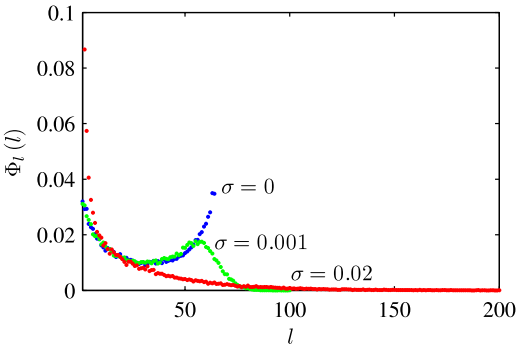

(b) $\varepsilon = 10^{-3}$, $\gamma = 1$, $\hat{x} = -0.05$, $\sigma_l = \sigma_r = \sigma$.

Fig. 8. Probability density of laminar lengths for map (2) with $a = 1$, $c = 0.05$ and the indicated values.

length with a good agreement with the numerical data. In these cases, the presence of noise modifies the shape of the probability density of the laminar lengths with respect to the expected form corresponding to the noiseless case. This behavior is also registered on the characteristic relation, which does not behave according to the position of the lower bound of reinjection, but its form depends on the LBR displaced by noise.

These results showed that although sometimes we can obtain analytical approaches for the statistical properties either for the noisy or noiseless system only using the noisy data, in some cases the presence of noise produces results that could be misinterpreted as they would be corresponding to a noiseless system, which could be particularly troublesome especially in case of handling experimental data.

On the other hand, when the noise is strong in the complete map, the results are approximately independent on the parameters of the map, the probability density of the laminar lengths always have the same shape and the saturation phenomenon is presented in the characteristic relation, i.e., the average laminar lengths reach a saturation value despite the position of the LBR point.

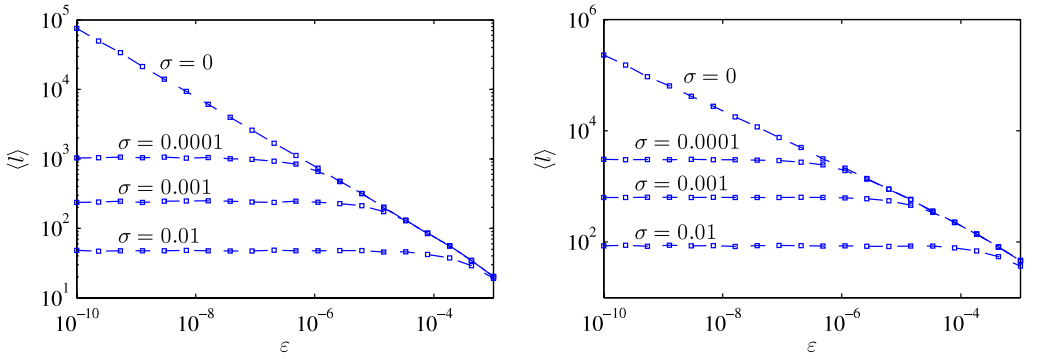

(a) $\hat{x} = -0.05$, $\gamma = 0.5$. (b) $\hat{x} = -0.05$, $\gamma = 2$.

Fig. 9. Characteristic relation $\langle l \rangle \propto \varepsilon^{\beta}$ for the map (2) with $a = 1$, $c = 0.05$ and the indicated values with $\sigma_l = \sigma_r = \sigma$. Squares indicate numerical data and the dashed line join the data reaching the corresponding saturation label for small values of ε.

Acknowledgments

This work has been supported by CONICET (Argentina) under Project PIP 11220090100809, by the Spanish Ministry of Science and Innovation under Project FIS2010-20054, and by grants of the National University of Córdoba and MCyT of Córdoba, Argentina.

References

[1] P. Manneville, Y. Pomeau, Intermittency and Lorenz model, Phys. Lett. A 75 (1979) 1–2.
[2] Y. Pomeau, P. Manneville, Intermittent transition to turbulence in dissipative dynamical system, Comm. Math. Phys. 74 (1980) 189–197.
[3] A. Nayfeh, B. Balachandran, Applied Nonlinear Dynamics, John Wiley & Sons Inc., New York, 1995.
[4] M. Dubois, M. Rubio, P. Berge, Experimental evidence of intermittencies associated with a subharmonic bifurcation, Phys. Rev. Lett. 51 (16) (1983) 1446–1449.
[5] J. Malasoma, P. Werny, M. Boiron, Multichannel type-I intermittency in two models of Raileigh–Bénard convection, Chaos Solitons Fractals 51 (15) (2004) 487–500.
[6] S. Stavrinides, A. Miliou, T. Laopoulos, A. Anagnostopoulos, The intermittency route to chaos of an electronic digital oscillator, Int. J. Bifurcation Chaos 18 (5) (2008) 1561–1566.
[7] G. Sanchez-Arriaga, J. Sanmartin, S. Elaskar, Damping models in the truncated derivative nonlinear Schrödinger equation, Phys. Plasmas 14 (2007) 082108.
[8] A. Chian, Complex system approach to economic dynamics, in: Lecture Notes in Economics and Mathematical Systems, Springer-Verlag, Berlin, Heidelberg, 2007, pp. 39–50.
[9] J. Zebrowski, R. Baranowski, Type I intermittency in nonstationary systems: models and human heart-rate variability, Physica A 336 (2004) 74–83.
[10] H. Schuster, W. Just, Deterministic Chaos, fourth ed., Wiley VCH, Mörlenbach, 2005.
[11] H. Kaplan, Return to type-I intermittency, Phys. Rev. Lett. 68 (1992) 553–557.
[12] T. Price, P. Mullin, An experimental observation of a new type of intermittency, Physica D 48 (1991) 29–52.
[13] N. Platt, E. Spiegel, C. Tresser, On–off intermittency: a mechanism for bursting, Phys. Rev. Lett. 70 (1993) 279–282.
[14] A. Pikovsky, G. Osipov, M. Rosenblum, M. Zaks, J. Kurths, Attractor–repeller collision and eyelet intermittency at the transition to phase synchronization, Phys. Rev. Lett. 79 (1997) 47–50.
[15] K. Lee, Y. Kwak, T. Lim, Phase jumps near a phase synchronization transition in systems of two coupled chaotic oscillators, Phys. Rev. Lett. 81 (1998) 321–324.
[16] A. Hramov, A. Koronovskii, M. Kurovskaya, S. Boccaletti, Ring intermittency in coupled chaotic oscillators at the boundary of phase synchronization, Phys. Rev. Lett. 97 (2006) 114101.
[17] A. Pikovsky, A new type of intermittent transtion to chaos, J. Phys. A: Math. Gen. 16 (1983) L109–L112.
[18] C. Kim, O. Kwon, E. Lee, H. Lee, New characteristic relation in type-I intermittency, Phys. Rev. Lett. 73 (4) (1994) 525–528.
[19] E. del Rio, S. Elaskar, New characteristic relation in type-II intermittency, Int. J. Bifurcation Chaos 20 (2010) 1185–1191.
[20] S. Elaskar, E. del Rio, J. Donoso, Reinjection probability density in type-III intermittency, Physica A 390 (2011) 2759–2768.
[21] E. Hirsch, B. Huberman, D. Scalapino, Theory of intermittency, Phys. Rev. A 25 (1) (1982) 519–532.
[22] E. Hirsch, M. Nauenberg, D. Scalapino, Intermittency in the presence of noise: a renormalization group formulation, Phys. Lett. A 87 (8) (1982) 391–393.
[23] W. Kye, S. Rim, C. Kim, J. Lee, J. Ryu, B. Yeom, Y. Park, Experimental observation of characteristic relations of type-III intermittency in the presence of noise in a simple electronic circuit, Phys. Rev. E 68 (3) (2003) 036203.
[24] A. Koronovskii, A. Hramov, Type-II intermittency characteristics in the presence of noise, Eur. Phys. J. B 62 (2008) 447–452.
[25] E. del Rio, M. Sanjuan, S. Elaskar, Effect of noise on the reinjection probability density in intermittency, Commun. Nonlinear Sci. Numer. Simul. 17 (2012) 3587–3596.
[26] E. del Rio, S. Elaskar, J. Donoso, Laminar length and characteristic relation in type-I intermittency, Commun. Nonlinear Sci. Numer. Simul. 19 (4) (2014) 967–976.
[27] E. del Rio, S. Elaskar, A. Makarov, Theory of intermittency applied to classical pathological cases, Chaos 23 (2013) 033112.
[28] G. Krause, S. Elaskar, E. del Río, Type-I intermittency with discontinuous reinjection probability density in a truncation model of the derivative nonlinear Schrödinger equation, Nonlinear Dynam. (2014) in press.